Electronic Supplementary Material (ESI) for Energy & Environmental Science.

Supplementary Information

Electro-synthesis of Ammonia from Nitrogen at Ambient Temperature and Pressure in Ionic Liquids

Fengling Zhou, Luis Miguel Azofra, Muataz Ali, Mega Kar, Alexandr N. Simonov, Ciaran McDonnell-Worth, Chenghua Sun, Xinyi Zhang and Douglas R. MacFarlane

1. Materials

Trihexyl(tetradecyl) phosphonium tris(pentafluoroethyl) trifluorophosphate ($[P_{6,6,6,14}]$[eFAP]) and 1-butyl-1-methylpyrrolidinium tris(pentafluoroethyl) trifluorophosphate ($[C_4mpyr]$[eFAP]) were purchased from Merck. N_2 used throughout was of High Purity grade from Air Liquide with specified content of H_2O 50 ppm and O_2 20 ppm. Ar was of High Purity grade from Air Liquide with specified H_2O content < 10 ppm and O_2 < 10 ppm. The trace amount of O_2 present in the gas streams was removed by an O_2 absorber column (Agilent).

The ionic liquid electrolytes (which are water immiscible) were pre-treated by washing with aqueous 1 mM KOH several times. The upper, aqueous phase was removed, and then the remaining IL phase was dried in a rotatory evaporator at 50 °C, followed by further drying under vacuum for 8 h. The dried ionic liquid was further dried by storing over molecular sieves. The dried ionic liquid then was transferred to a vial through which N_2 was bubbled (10 mL min^{-1}) for at least 12 h to fully equilibrate the liquid with respect to N_2 and H_2O before use in experiments. For Ar control experiments the gas stream was replaced with Ar. Water content was measured by Karl Fisher titration; 100 ± 10 ppm was typically achieved after equilibration and used in all experiments, unless otherwise specified. In some cases additional water was added by micropipette. Where a lower water content was required, a H_2O-free gas stream was achieved by passing over a molecular sieves column and controlled mixing with the primary gas supply.

Electrochemical N_2 reduction was conducted in a three-electrode configuration with N_2 gas flowing over the working electrode as shown in Figure S1. A Biologic VMP electrochemical workstation was used in all experiments. Cyclic voltammograms were measured in a single compartment cell, while ammonia production at fixed potential was conducted by isolating the platinum counter electrode with a glass frit in a typical H-cell arrangement.

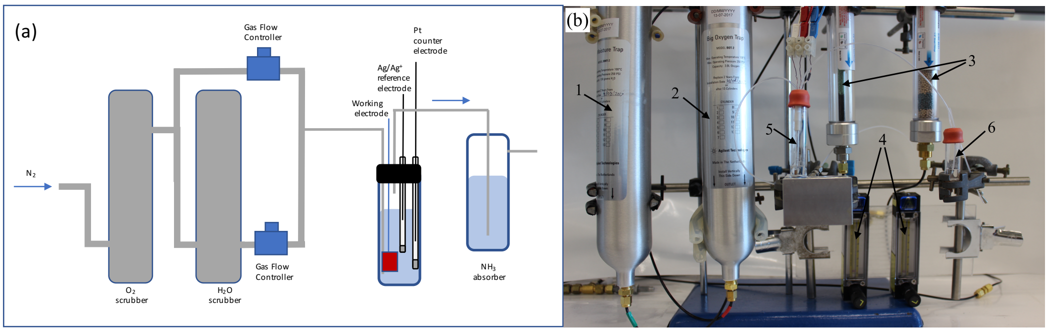

Figure S1. (a) Schematic of experimental set-up; (b) Photograph of experimental set-up showing the gas pre-treatment line and electrochemical cell: 1) moisture trap (Agilent); 2) O_2 trap (Agilent); 3) O_2 and moisture indicators; 4) gas flow controllers; 5) electrochemical cell sitting on the top of its heating block (normally inserted during experiments); 6) NH_3 absorber (1mM H_2SO_4).

Several working electrode substrates were investigated, including fluorine doped tin oxide glass (FTO, TEC8 from Dyesol), nickel foam (NF, Sigma-Aldrich), stainless steel (SS) mesh (400 mesh, 0.03 mm wire with 0.034 mm opening from Dancore Pty). The substrates were washed by sonication in water for 5 min, then in ethanol for 5 min, and washed with fresh ethanol followed by drying with N_2 gas before electro-deposition.

The synthesized ammonia was transferred from the reaction vessel by the gas stream, to a trap containing a weak aqueous acid solution (1 mM H_2SO_4) which was later analyzed. Any ammonia remaining in the ionic liquid was extracted from the water-immiscible IL by washing with 1 mM aqueous KOH; this extract was combined with the trap solution for analysis. Ammonia was quantified using the indophenol blue method; limit of detection of the method is estimated to be 1 nmol under the conditions of the experiments conducted here.

The Faradaic efficiency was calculated based on the 6-electron process ($N_2 + 6e^- + 6H_2O \rightarrow 2NH_3 + 6OH^-$). H_2 was measured using a pre-calibrated gas chromatograph, and the Faradic efficiency for H_2 calculated based on the 2-electron process. The products were also analyzed for the presence of hydrazine, an intermediate in N_2

reduction, but no significant levels were found. The main by-product was H_2 produced *via* the hydrogen evolution reaction ($2H_2O + 2e^- \rightarrow H_2 + 2OH^-$).

We have carefully analyzed our high purity N_2 gas supply by flow injection analysis techniques to determine (i) the NH_3 and (ii) NO_x species in the gas. The limit of detection of the technique is 1ppb in both cases.

To do this analysis we have passed large volumes of gas through our collector vials to trap the impurities in the gas stream. We used a second collector vial in the chain to confirm that all of the impurities have been absorbed in the first vial. From this we determined that the gas stream contains at most 0.4 vppm NO_x and 0.003 vppm NH_3.

In regard to ammonia contamination from the gas stream, the total amount therefore present in the volume of gas used in our typical NRR experiment is calculated to be only 0.15 nmol. This can be compared to reaction yields of 10 – 50 nmol that are presented in the paper. Note also that control experiments using Ar demonstrate that no ammonia is present in the IL, or produced during electrolysis in the absence of the N_2 gas supply. So we conclude that direct ammonia contamination from the gas stream (or the collector solutions or the IL) is not significant in our experiments.

To assess the impact of the NO_x present in the gas stream we carried out the following control experiment. We passed excess (50L) of the N_2 supply through 20 mL of the IL in order to saturate the IL with NO_x related species. Subsequent analysis of the IL indicates an accumulated nitrate/nitrite impurity concentration of 6 nmol/mL. If we assume that all of this could potentially be reduced during our typical NRR experiment (which involves 1 mL of IL), then we could expect to find a maximum 6 nmol of NH_3 from this source. This is substantially lower than the ammonia yield (16 ± 1 nmol) produced from the electrochemical reaction carried out with this sample (no further gas supplied) and therefore the results reported here cannot result from NO_x reduction alone. We therefore can conclude that NRR is taking place in our experiments as the dominant process.

We have not subtracted this potential background off from our results, since the actual reduction of the NO_x species in our experiments has not been proven. It is difficult to construct an experiment to prove this NO_x process is actually occurring (at this low level of reactant).

Note that, since nitrate/nitrite reduction requires 8/7 electrons per N to reduce to ammonia, our Faradaic Efficiency results are, if anything, under-estimates of the true NRR FE, should small amounts of NOx also be reduced.

Ar gas used in control experiments was also analysed; NO_x was below the detection limit (1vppb) and NH_3 was 0.06vppm.

2. Reference electrode preparation and calibration

The Ag/Ag^+ reference electrode, well known in ionic liquid electrochemistry, was used; this was calibrated by use of the ferrocene/ferrocenium couple and potentials were then converted to the normal hydrogen electrode (NHE) scale (Figure S2). Silver trifluoromethanesulfonate was used as the source of Ag^+ ions, and dissolved in a small amount of [C_2mim][BF_4], followed by addition of [C_4mpyrr][eFAP] to make a 10 mM Ag^+ electrolyte. The prepared electrolyte was then filled into a fritted Ag reference electrode assembly. The Ag/Ag^+ electrode potential was calibrated (Figure S2) by using the ferrocene/ferrocenium (Fc/Fc^+) couple in [C_4mpyr][eFAP].[1] This was converted to the NHE scale on the basis that $E^0(Fc^{0/+})$ = 0.64 V vs normal hydrogen electrode (NHE). All potentials are reported *vs.* NHE, while all currents are normalized to the geometric surface area of the electrode.

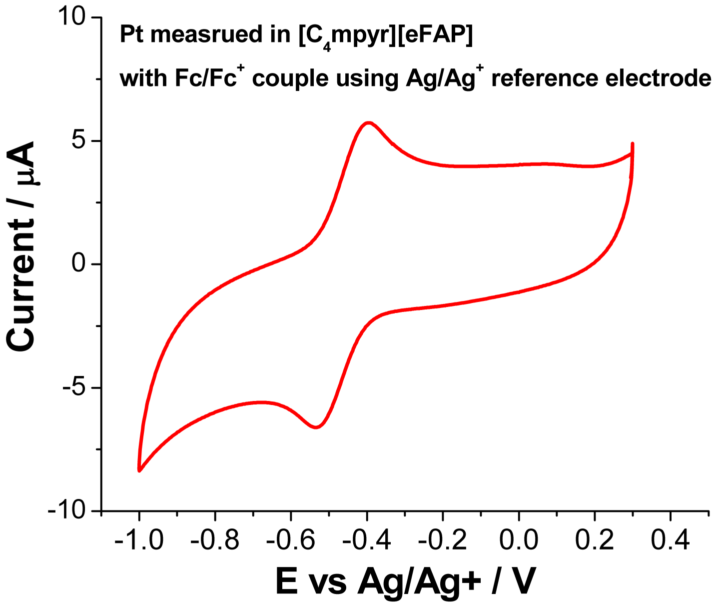

Figure S2. Cyclic voltammetric calibration of the Ag/Ag^+ reference electrode vs. the $Fc^{0/+}$ redox couple.

3. Preparation and Characterization of Fe Electrocatalyst

Fe-based catalytic layers on the substrates were prepared by electro-deposition using a VMP potentiostat in a three-electrode configuration. A saturated calomel reference (SCE) electrode and a high surface area Ti mesh served as the reference and counter electrode, respectively. The deposition solution contained 10 mM $FeSO_4$, 10 mM NaOH and 10 mM citric acid in water. Typically, electro-deposition was conducted by cycling the potential between -1.8 V and -0.8 V at a sweep rate of 0.02 V s^{-1}, which produced a black film only after several cycles. Such a deposition strategy produces small particles of 2 – 10 nm in diameter that form nanostructured layers of the Fe-based catalyst. On the otherhand, standard potentiostatic electro-deposition was found to produce more dense layers of larger particles, *i.e.* a smoother surface with lower electro-catalytic activity.

The Fe phase composition of the electro-catalyst film was characterized by X-Ray diffraction (XRD). The XRD pattern, as shown in Figure S3, exhibits a peak at $2\theta = 45°$, which corresponds to the (110) plane of the *bcc* phase of Fe metal.

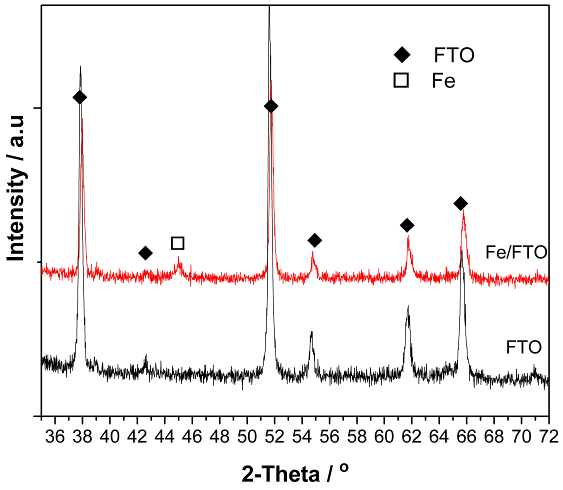

Figure S3. The XRD pattern of the electrodeposited Fe film on FTO glass.

The amount of Fe deposited was measured by titration with potassium permanganate. In detail, the sample of Fe catalyst (electrode geometric area = 0.25 cm^2) was firstly dissolved in 5 mL of 10 mM H_2SO_4, and this was titrated by adding 0.001 M potassium permanganate solution. Preliminary optimisation of the loading indicated that the Fe catalyst prepared by 5 cycles, which deposits 146 ± 7 $\mu g\ cm^{-2}$, produced the highest FE.

The electrochemically active surface area (ECSA) and the roughness factor (RF) of the electrodes were estimated from the double layer capacitance, which was derived from cyclic voltammetry using a literature procedure[2] and as shown in Figure S4. The measured double layer capacitance (C_{DL}) of SS and Fe/SS were 0.09 mF cm^{-2} and 0.36 mF cm^{-2}, respectively, and the RF's were calculated as 2.2 and 9, respectively.

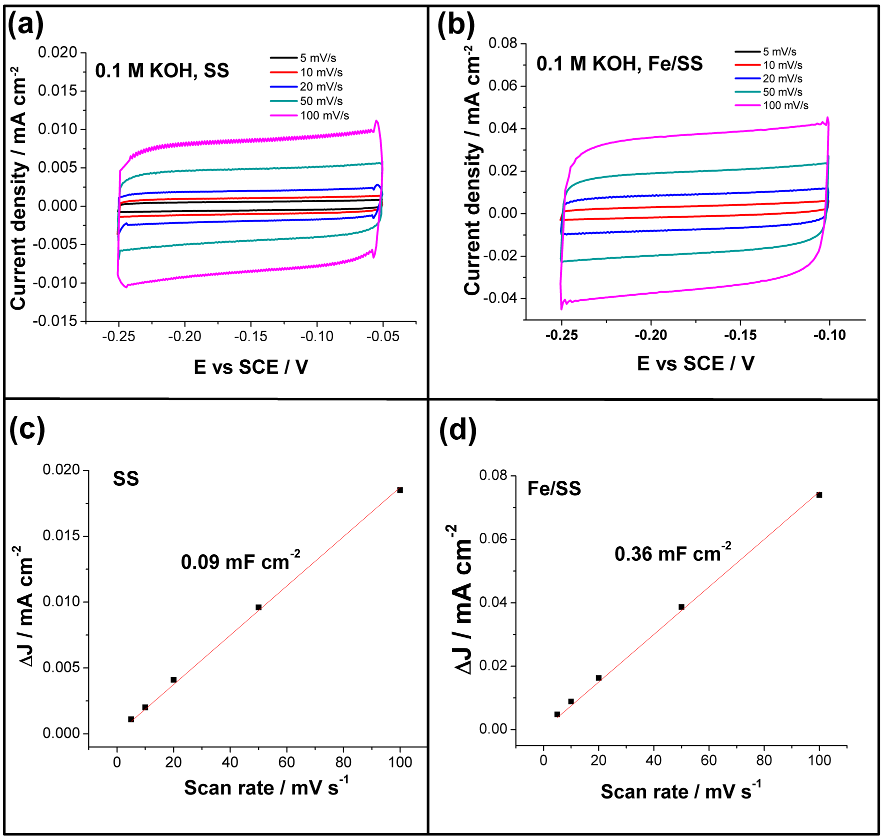

Figure S4. Cyclic voltammograms obtained for the (a) SS and (b) Fe-SS electrodes in contact with Ar-purged 0.1 M KOH at different scan rates, and dependence of the difference in forward and backward sweep current densities at –0.15 V on the scan rate for (c) SS and (d) Fe-SS.

4. Electrochemical Performance

Temperature Dependence

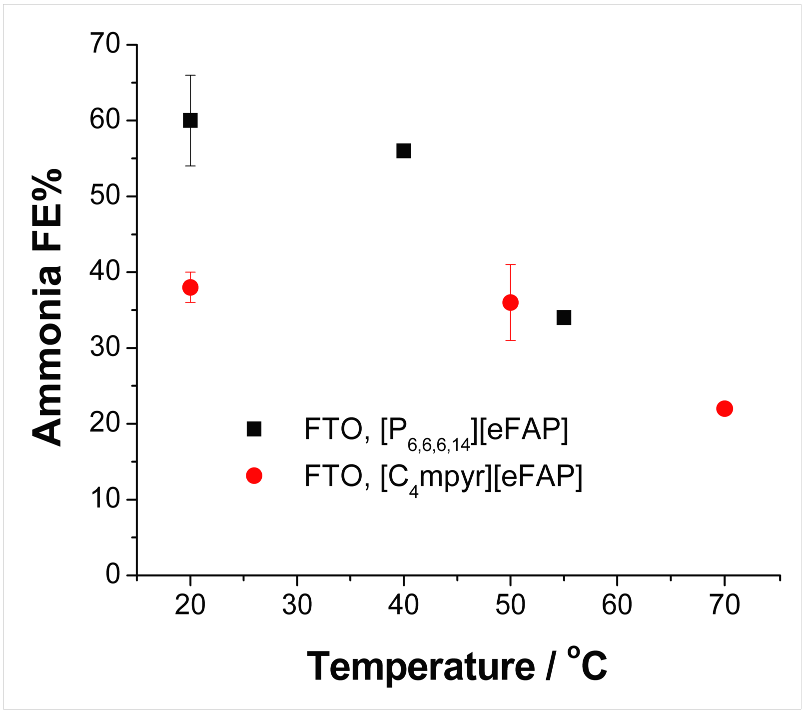

Figure S5. Temperature dependence of faradic efficiency for N_2 reduction on Fe-FTO in $[P_{6,6,6,14}]$[eFAP] (black squares: measured on the same electrodes in sequence of 20°C, 40°C, 55 °C) and $[C_4mpyr]$[eFAP] (red circles, measured on the same electrodes in sequence of 50°C, 70 °C, 20 °C) at –0.8 V *vs*. NHE.

NRR at different water contents

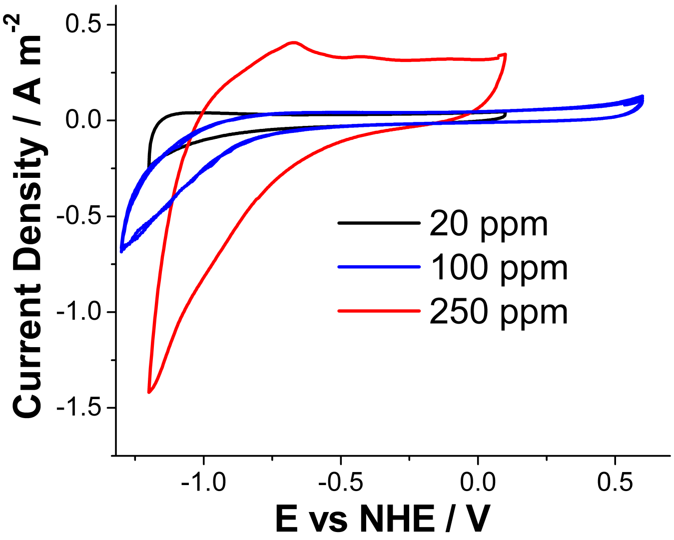

Figure S6. Cyclic voltammograms measured on Fe-FTO at scan rate of 2 mV s^{-1} in ionic liquid $[C_4mpyr]$[eFAP] containing different concentrations of H_2O.

Yield versus Time

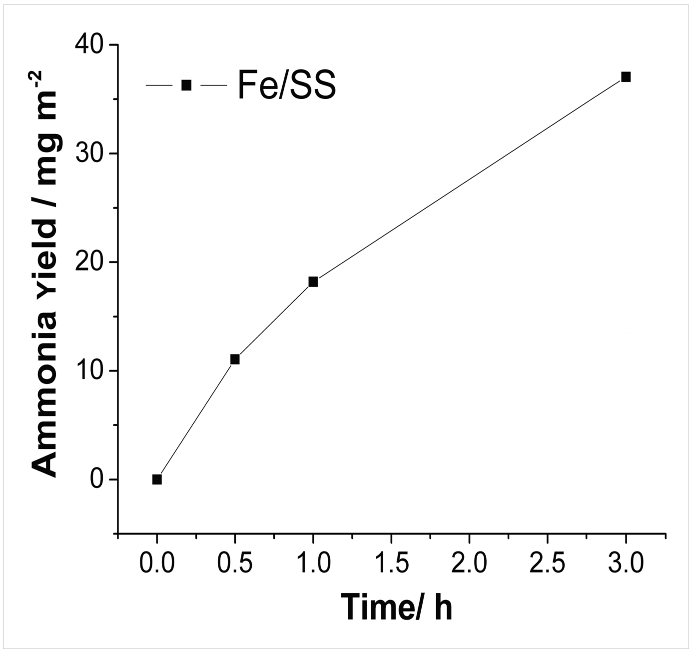

Figure S7. The dependence of yield of ammonia on electrolysis time of the N_2-saturated $[P_{6,6,6,14}]$[eFAP] using the Fe-SS electrode at -0.8 V.

5. Viscosity Data

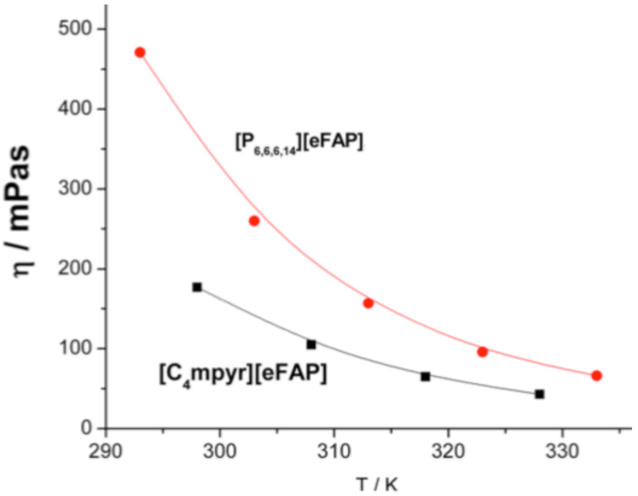

Figure S8. Comparison of the viscosity of the two ionic liquids used in this study. The viscosity of $[C_4mpyr]$[eFAP] was measured using a microviscometer (Anton Paar, Lovis 2000 M). The data for $[P_{6,6,6,14}]$[eFAP] is reproduced from Ref.3 [3]

6. N_2 isotope labelling experiment

Labelled $^{15}N_2$ gas purchased from Sigma was used to further confirm that the ammonia produced is from the N_2 gas supplied to the experiment. We found the small, 1 L, cylinders (Sigma-Aldrich, SKU No: 364584-1L) to be ultimately an in-efficient choice because the pressure drops so rapidly in these cases and a substantial fraction of the volume of gas becomes un-usable. Instead we used the 5 L cylinders (Sigma-Aldrich, SKU No: 364584-5L) to complete the experiments. The gas was pre-purified by passing through acid solution (1 mM H_2SO_4) followed by distilled water traps to remove any NO_x and NH_3 contamination in the $^{15}N_2$. The ammonia produced was quantified by using an ^{1}H-NMR measurement on a Bruker NMR600 as follows. The ^{1}H NMR signal of $^{15}NH_4^+$ is split by the nuclear spin of ^{15}N into a well-known doublet (~73 Hz) in the region near 7.0 ppm, while ^{14}N produces a triplet (~52 Hz) in the same region.[4-6] The signals are of different sensitivity.[4, 7] The $^{15}NH_4^+$ signal at 7.04 ppm sits clear of any interfering signals, including that of $^{14}NH_4^+$, and is suitable for quantification. A calibration curve, Figure S9a, was obtained for the integration of this signal as a function of concentration using standard solutions made up from $^{15}NH_4Cl$ (from Sigma) dissolved in 0.01 M HCl. A known quantity of d^6-DMSO was added as an internal standard. Spectra obtained for the calibration samples are shown in Figure S9c. Similarly, $^{14}NH_4^+$ can be quantified from its signal at 6.99 ppm and a calibration curve was also obtained for this signal (Figure S9a) using $^{14}NH_4Cl$. All experiments were undertaken with water suppression and 8000 scans (except the 100μM $^{15}NH_4Cl$ sample, which required only 1000).

In the $^{15}N_2$ reduction experiment, a standard experiment was carried out using an Ar purge to remove $^{14}N_2$ and then purging for 30 min with $^{15}N_2$. Other standard experimental details were as described in the main paper, or in sections 1-3 above. The ammonia produced was extracted from the ionic liquid electrolyte using de-ionized water, and then the pH of the extract was adjusted to 2 by adding 1M HCl. A known quantity of d^6 - DMSO was added as an internal standard. The spectrum obtained is shown in Figure S9b, indicating peaks from both $^{15}NH_4^+$ and $^{14}NH_4^+$. Some amount of the latter is to be expected given the difficulty in completely eliminating $^{14}N_2$ from the $^{15}N_2$ experiment. The $^{15}NH_4^+$ and $^{14}NH_4^+$ products quantified by this method were 15±2.4 nmol and 5.5±0.5 nmol respectively. The total of these, 20±3 nmol, is approximately as expected on the basis of a sample from a parallel experiment analysed by the indophenol method, which produced 19±2 nmol. To check for any possible cross-interference effects, an NMR spectrum of a solution that contained concentrations of $^{15}NH_4Cl$ and $^{14}NH_4Cl$ similar to the experimental sample was recorded and is shown in Figure S9b. Thus, these experiments indicate that the $^{15}N_2$ reduction reaction was substantially the principal source of the NH_3 produced in this experiment.

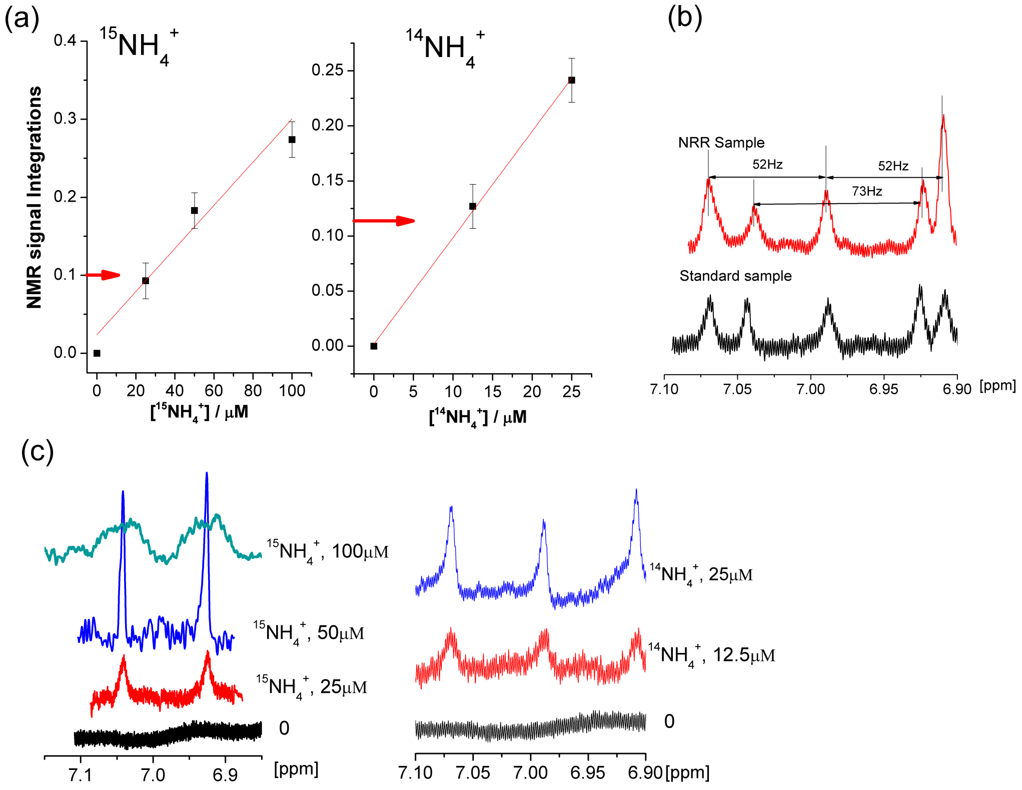

Figure S9. a) Peak area calibration curves of the ^{1}H NMR signal at 7.04 ppm for standard solutions of $^{15}NH_4Cl$ and the peak at 6.99 ppm for standard solutions of $^{14}NH_4Cl$; arrows indicate the NMR measurement obtained for the $^{15}N_2$ reduction sample in each case. Note that the scale is μmol/L and sample volume in the NMR experiment was 0.3 mL; b) ^{1}H NMR spectra of the $^{15}N_2$ reduction sample (in red) demonstrating the formation of $^{15}NH_4^+$ after electrolysis; also shown (in black) is a spectrum from a sample made up to contain 8 nmol (=16μM) $^{15}NH_4Cl$ and 6.5 nmol (=13μM) $^{14}NH_4Cl$; c) spectra for the $^{15}NH_4Cl$ and $^{14}NH_4Cl$ calibration solutions.

7. Computational Details

Calculations on the N_2 interactions with (i) anions, (ii) cations and (iii) ion-pairs were conducted by means of Density Functional Theory (DFT) using the M06-2X[8] functional developed by Truhlar and co-workers and double-ζ Pople's 6-31+G(d) basis set,[9] which includes diffusion and polarization functions for all heavy atoms. The EDIIS/CDIIS procedure[10] was applied for the self-consistent field (SCF) in all cases. Also, in order to confirm the nature of the stationary points and to obtain Zero-Point Energy (ZPE) corrections, frequency calculations were performed for all the models. The Polarisable Continuum Model (PCM) was also employed to implicitly emulate the solvent with the standard parameters programmed for tetrahydrofuran.[11]

All the energy calculations were carried out within the facilities provided by the Gaussian09 package (revision D.01).[12] Electronic binding energies were computed as the difference between the optimised complexes and the optimised monomers, including ZPE.

Binding energies were calculated from $\Delta E = E_{complex} - E_{ion/ionpair} - E_{N2}$ including vibrational zero point energies.

References

1. Deng, P.; Liu, L.; Ren, S.; Li, H.; Zhang, Q. *Chemical Communications* **2012,** 48, (55), 6960-6962.
2. McCrory, C. C. L.; Jung, S.; Ferrer, I. M.; Chatman, S. M.; Peters, J. C.; Jaramillo, T. F. *J. Am. Chem. Soc.* **2015,** 137, (13), 4347-4357.
3. Stevanovic, S.; Gomes, M. F. C. *J. Chem. Thermodynamics* **2013,** 59, 65-71.
4. Liu, J.; Kelley, M. S.; Wu, W. Q.; Banerjee, A.; Douvalis, A. P.; Wu, J. S.; Zhang, Y. B.; Schatz, G. C.; Kanatzidis, M. G. *Proc. Natl. Acad. Sci. U. S. A.* **2016,** 113, (20), 5530-5535.
5. Bobtoff, S.; Philips, R. J.; Shekarriz, A. Nuclear Magnetic Resonance Measurement of Ammonia Diffusion in Dense Solid-Liquid Slurries*, Report to U. S. Department of Energy,* **1998**.
6. Preece, N. E.; Cerdan, S. *Analytical Biochemistry* **1993,** 215, (2), 180-183.
7. Wickramasinghe, L. A.; Ogawa, T.; Schrock, R. R.; Müller, P. *J. Am. Chem. Soc.* **2017,** 139, (27), 9132-9135.
8. Zhao, Y.; Truhlar, D. G. *Theoretical Chemistry Accounts* **2008,** 120, (1), 215-241.
9. Frisch, M. J.; Pople, J. A.; Binkley, J. S. *The Journal of Chemical Physics* **1984,** 80, (7), 3265-3269.
10. Kudin, K. N.; Scuseria, G. E.; Cancès, E. *The Journal of Chemical Physics* **2002,** 116, (19), 8255-8261.
11. Tomasi, J.; Mennucci, B.; Cammi, R. *Chemical Reviews* **2005,** 105, (8), 2999-3094.
12. Frisch, M. J. T., G. W.; Schlegel, H. B.; Scuseria, G. E.; Robb, M. A.; Cheeseman, J. R.; Scalmani, G.; Barone, V.; Mennucci, B.; Petersson, G. A.; Nakatsuji, H.; Caricato, M.; Li, X.; Hratchian, H. P.; Izmaylov, A. F.; Bloino, J.; Zheng, G.; Sonnenberg, J. L.; Hada, M.; Ehara, M.; Toyota, K.; Fukuda, R.; Hasegawa, J.; Ishida, M.; Nakajima, T.; Honda, Y.; Kitao, O.; Nakai, H.; Vreven, T.; Montgomery Jr., J. A.; Peralta, J. E.; Ogliaro, F.; Bearpark, M.; Heyd,

J. J.; Brothers, E.; Kudin, K. N.; Staroverov, V. N.; Kobayashi, R.; Normand, J.; Raghavachari, K.; Rendell, A.; Burant, J. C.; Iyengar, S. S.; Tomasi, J.; Cossi, M.; Rega, N.; Millam, N. J.; Klene, M.; Knox, J. E.; Cross, J. B.; Bakken, V.; Adamo, C.; Jaramillo, J.; Gomperts, R.; Stratmann, R. E.; Yazyev, O.; Austin, A. J.; Cammi, R.; Pomelli, C.; Ochterski, J. W.; Martin, R. L.; Morokuma, K.; Zakrzewski, V. G.; Voth, G. A.; Salvador, P.; Dannenberg, J. J.; Dapprich, S.; Daniels, A. D.; Farkas, Ö.; Foresman, J. B.; Ortiz, J. V.; Cioslowski, J.; Fox, D. J. Gaussian, Inc.: Wallingford CT, 2009.